Journal of Robotics and Control (JRC)
Volume 5, Issue 2, 2024
ISSN: 2715-5072, DOI: 10.18196/jrc.v5i2.21227

Improving the Efficiency of Open Cathode PEM Fuel Cell Through Hydrogen Flow Control Using Wavelet-Clipping

Triyanto Pangaribowo [1*], Wahyu Mulyo Utomo [2], Abdul Hamid Budiman [3], Deni Shidqi Khaerudini [4], Afarulrazi Abu Bakar [5]
[1] Department of Electrical Engineering, Faculty of Engineering, Universitas Mercu Buana, Jakarta Indonesia, Indonesia
[1, 2, 5] Faculty of Electrical and Electronic Engineering, University Tun Hussein Onn Malaysia, Johor, Malaysia
[3] Research Center for Energy Conversion and Conservation, National Research and Innovation Agency (BRIN), Bld. 440 Kawasan Puspiptek Serpong, South Tangerang, 15314 Banten, Indonesia
[4] Research Center for Advanced Materials, National Research and Innovation Agency (BRIN), Bld. 440 Kawasan Puspiptek Serpong, South Tangerang, 15314 Banten, Indonesia
Email: [1] triyanto.pangaribowo@mercubuana.ac.id, [2] wahyu@uthm.edu.my, [3] abdu031@brin.go.id, [4] deni.shidqi.khaerudini@brin.go.id, [5] afarul@uthm.edu.my
*Corresponding Author

***Abstract*—Open cathode proton exchange membrane fuel cells (OC-PEMFC) are devices that produce electrical energy through an electrochemical reaction between hydrogen and oxygen gas. Rapid load changes often lead to fluctuations in the flow of hydrogen entering the OC-PEMFC system. Increased load directly correlates with higher hydrogen gas consumption. However, if there is a delay in adjusting the gas flow rate to changes in load, it can trigger fluctuations in the amplitude and frequency of the output voltage. This fluctuation ultimately disrupts the stability of the power supply to the load, and reducing efficiency. Therefore, this paper presents a novel hybrid system that integrates wavelet and clipping techniques to regulate a more stable hydrogen flow, enhancing efficiency and accuracy under constant load conditions. A wavelet control system is used to mitigate noise, coupled with amplitude limitation through clipping techniques. This control system is implemented in OC-PEMFC model that is validated with experimental data. The performance analysis of this hybrid system reveals a 1.95 % increase in efficiency and attains high accuracy, as evidenced by a low ISE value of 0.028 during interference.**

Keywords—OC-PEMFC; Efficiency; Hydrogen Flow Control; Wavelet; Clipping.

I. INTRODUCTION

Fuel cell system generally has the potential to serve as an energy source for the future due to its environmentally-friendly characteristics [1][2][3]. It generate electrical energy by means of a chemical reaction between oxygen and hydrogen gas [4][5]. Hydrogen, being a renewable energy source with minimal environmental impact, demands efficient utilization [6][7][8]. Achieving a higher fuel cell system efficiency involves managing all sub-systems optimally [9][10], including the flow of hydrogen gas [11][12].

The electrical output of a PEM fuel cell relies on the quantity of hydrogen and oxygen engaging at the electrodes, generating electricity and water as byproducts [13][14]. The adjustment of the hydrogen flow rate allows for the regulation of the power output [15][16][17]. Augmenting the flow rate will lead to increased power output, whereas reducing the flow rate will yield a decrease in power output [18][19]. PEM fuel cell commonly employ a control mechanism that modulates hydrogen flow in response to power requirements, ensuring consistent power output and maximizing efficiency [20][21][22].

Open cathode PEM fuel cells (OC-PEMFC) exhibit the feature of drawing oxygen into the cathode channel directly from the air using fans [23][24]. The benefits encompass a simple design, cost-effectiveness, and minimal parasitic loss [25], rendering them widely applicable in electric vehicles, residential, and stationary energy systems [26]. However, challenges emerge during increased loads, potentially leading to fluctuation issues [27]. Rapid load changes, without corresponding adjustments to hydrogen flow, induce amplitude and frequency variations in the output voltage [28]. Therefore, it is crucial to maintain the stability of the hydrogen flow to ensure a stable power supply to the load [29][30].

Numerous studies have investigated fuel cell performance through various methods, including experimentation, theoretical analysis, modeling, and simulation. These studies reveal that fuel cell efficiency is significantly impacted by the stability of gas flow, crucial for achieving optimal performance [31]. Performance degradation often occurs under load due to a delay in gas flow rate adjustment [32][33]. Effective management of gas distribution promotes higher power density and output voltage stability [34][35][36]. Instabilities in hydrogen gas supply lead to fuel cell performance deterioration[37]. While several methods, such as proportional-integral(PI) controller [22], fuzzy control [38], Hybrid fuzzy PID [39][36], and PI controller with PSO method [40] have been proposed to enhance fuel cell performance by regulating hydrogen flow, they exhibit limitations in highly dynamic systems like fuel cell generators. The application of PID control faces

challenges when dealing with non-linear systems characterized by high dynamics [41]. Similarly, fuzzy controllers present difficulties as they can result in suboptimal control performance, impacting both accuracy and stability [42].

In this paper, we introduce a hybrid wavelet-clipping method designed to regulate hydrogen flow in OC-PEMFC. The primary novelty of this paper resides in introducing a novel method specifically designed for use in OC-PEMFC. The proposed method strives to enhance fuel cell efficiency by refining the accuracy and stability of both hydrogen flow and voltage output. It achieves this goal through the application of wavelet transform to reduce noise and clipping techniques to limit high amplitudes. The control system integrated into the fuel cell model has undergone validation using experimental data to ensure model accuracy. The structure of this paper is as follows: Section II elaborates on the fuel cell mathematical equations, experimental setup, and the proposed control system. Section III presents the experimental results and discussion, while Section IV concludes this paper.

II. RESEARCH METHODOLOGY

This section presents the mathematical equations relevant to a fuel cell, as well as the experimental setup used to obtain analytical results and details the proposed control system.

A. Mathematical Equations of Fuel Cell

Mathematical models for fuel cells encompass both static and dynamic representations. Static models offer a depiction of a fuel cell system in a steady state, describing its behavior under constant operating conditions without accounting for transient changes or variations over time. On the other hand, dynamic models incorporate temporal aspects and simulate changes in the system, such as fluctuations in hydrogen gas flow and load.

Static model of fuel cell:

Typically, the output of a fuel cell system manifests as voltage, with its output influenced by various factors that contribute to voltage drops [43]. Equation (1) describes the various voltage loss factors, such as activation loss (V_{Act}), ohmic loss(V_{Ohmic}), and concentration loss(V_{con}) [44][45], that impact the voltage drop in the fuel cell output [46].

$$V_{FC} = N_{cell}(E_{Nernst} - V_{Act} - V_{Ohmic} - V_{con}) \quad (1)$$

In this case, N_{cell} represents the total quantity of cells, amounting to 73 and E_{Nernst} represents the reversible electric potential [47][48], determined using the equation (2).

$$E_{Nernst} = E^0 + \frac{RT}{2F}[\ln(P_{h_2}) + 0.5\ln(P_{o_2}) \quad (2)$$

Here, E^o is the reference potential [49]set at 1.229 V, R denotes the universal gas constant (8.314 J/mol K) [50], T signifies the fuel cell operating temperature (333 K), and F represents the Faraday constant (96485 C/mol) [51]. The voltage drop (V_{act}) attributed to activation in both the anode and cathode [52][53] is computed using equation (3).

$$V_{act} = -\left(\frac{R \times T}{2 \times \alpha \times F}\right) \times \log\left(\frac{i_L}{i_0}\right) \quad (3)$$

Where α is a transfer coefficient set at 0.5, i_L represents the limiting current density at 1.4 A/cm², and an exchange current density (i_0) is specified as 10^-6.912 A/cm². The ohmic overpotential represents the loss attributed to the resistance of cell components [54][55]. The estimation of ohmic losses (V_{ohmic}) [56] is calculated using Ohm's law.

$$V_{ohmic} = -(i_o \times r) \quad (4)$$

The internal resistance (r) is assigned a value of 0.19 Ohm-cm². The voltage drop arising from mass transport effects, impacting the concentration of reacting gases, is represented as V_{conc} [57][58]and is calculated using equation (5).

$$V_{con} = -\alpha \times i^k \times \ln\left(1 - \frac{i_o}{i_l}\right) \quad (5)$$

Where k represents the constant utilization set at the value 1.1.

Dynamic model of fuel cell:

The dynamics of this model rely on the correlation between the output voltage and the partial pressures of hydrogen, oxygen, and current. The correlation between the molar flow of hydrogen gas through the valve and its partial pressure in the line can be represented as K_{H2} [59]. Equation (6) can be employed to calculate K_{H2}.

$$K_{H_2} = \frac{qH_2}{PH_2} = \frac{k_{an}}{\sqrt{MH_2}} \quad (6)$$

The molar constant for the hydrogen valve (K_{H2}) is specified as 0.843 mol/s.atm. In this context, the symbol qH_2 corresponds to the molar flow of hydrogen, and PH_2 represents the partial pressure of hydrogen [60]. Additionally, MH_2 stands for the molar mass of hydrogen [61], and K_{an} represents the anode valve constant. Equation (7) facilitates the calculation of the reactive hydrogen flow, denoted as $q^r_{H_2}$.

$$q^r_{H_2} = \frac{N_{cell} \cdot I_{stack}}{2F} = 2K_r \quad (7)$$

Here, K_r represents the modeling constant [62] with a value of 1.4251×10-6 kmol s^{-1} A^{-1}.

$$K_r = \frac{N_{cell}}{4F} \quad (8)$$

The mathematical equation for the partial pressure of hydrogen gas, represented by the symbol PH_2 [63][64] is as follows:

$$P_{H_2} = \frac{\frac{1}{K_{H_2}}}{1 + \tau H_2 s}\left(q^{in}_{H_2} - 2K_r I_{stack}\right) \quad (9)$$

Here, I_{stack} represents the stack current. The symbol $q_{H_2}^{in}$ signifies the input hydrogen flow rate, and τH_2denotes the hydrogen time constant [65] with a value of 3.37 seconds. The calculation of τ_{H_2} is determined by the equation (10) [66][67].

$$\tau_{H_2} = \frac{V_{an}}{K_{H_2} RT} \tag{10}$$

The symbol V_{an} denotes the volume of the anode (m^3) [68]. Equation (11) enables the calculation of the partial pressure of oxygen gas at the cathode of the fuel cell (P_{O_2}) [66][67].

$$P_{O_2} = \frac{{}^1/_{K_{O_2}}}{1 + \tau_{O_2}} \left(q_{O_2}^{in} - K_r I\right) \tag{11}$$

The valve constant for oxygen (K_{O_2}) is 2.52 mol/s.atm, and the oxygen time constant (τ_o) has a value of 6.74 seconds. Equation (12) facilitates the calculation of the molar flow of hydrogen gas (q_{H_2}) [50].

$$q_{H_2} = \frac{N_0 I_{stack}}{2FU} \tag{12}$$

The total fuel cell voltage (V_{FC}) is computed through the following equation [69].

$$V_{FC} = V_{cell} N_{cell} \tag{13}$$

Where V_{cell} is the OC-PEMFC stack voltage.

B. Experimental Setup

The experimental setup utilized OC-PEMFC specifications (Fig. 1 and Fig. 2), featuring cell dimensions of 34 cm × 7 cm with a thickness of 4 mm and an active area of 5.5 cm × 29 cm. Despite the fuel cell's maximum power output capacity of 2.5 kW, the experiment imposed a restriction, capping the maximum power at 300 W due to device limitations.

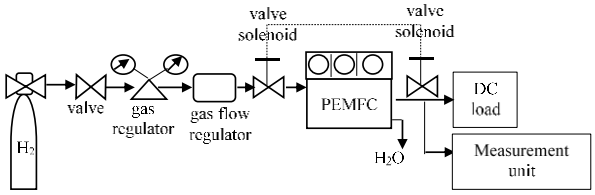

Fig. 1. Block diagram of OC-PEMFC testing

Fig. 1 provides a schematic representation of the experimental setup in this study. The experimental apparatus included an open cathode type PEM fuel cell, a gas regulator, a flowmeter, a fan, a DC power supply, a DC load, and devices for measuring power, current, and voltage.

Hydrogen for the fuel cell was supplied from a pressurized gas cylinder regulated by a pressure-reducing regulator that controlled the gas flow rate. The fuel cell's output was monitored using a DC voltage monitoring tool, while current and power were measured using corresponding monitoring tools. Tests were conducted at a minimum operating temperature of 31°C.

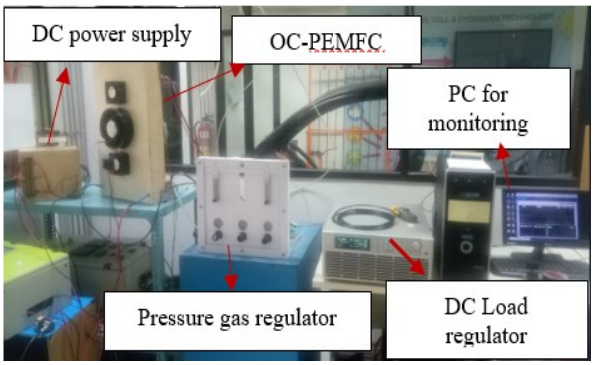

Fig. 2. Experimental set up of OC-PEMFC

In this experiment, a hydrogen flow of 8 L/min was used as the input. The initial phase involved heating the OC-PEMFC for 30 minutes without connecting it to a load. The stable maximum voltage measured without a load was 76.446 volts. Subsequently, the OC-PEMFC was connected to a load with a current ranging from 1 A to 10 A, and the results were observed through a monitoring system. The measured voltage and current data were utilized to generate a curve, which will be employed for model validation and to analyze the power produced by the OC-PEMFC.

C. Control System Structure

The proposed control system creatively combines clipping and wavelet techniques to manage hydrogen flow in fuel cells. In the control system, the set point represents a current serving as both a feedforward input and a reference for the desired or sustained target value. Feedforward, integral to the control strategy, directly counteracts disturbances or alterations impacting the system's output. Fig. 3 illustrates the feedback and feedforward control structures utilized in this hybrid system. The experimental results indicate that significant fluctuations emerge when the current load reaches 6.9 A and beyond. Therefore, for the implementation of this control system, a setpoint value of 6.9 A is recommended.

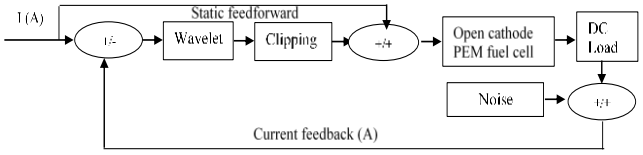

Fig. 3. Control system structure

Matlab Simulink was utilized to create both static and dynamic models based on the mathematical equations of fuel cells. These models simulate OC-PEMFC, illustrating the relationship between output voltage and the partial pressures of hydrogen and oxygen. Following that, the control system is implemented within the OC-PEMFC model, which was constructed using Matlab software, illustrated in Fig. 4. The simulation model, constructed using Matlab Simulink, is derived from general fuel cell mathematical equations and subsequently validated with experimental data to ensure its accuracy.

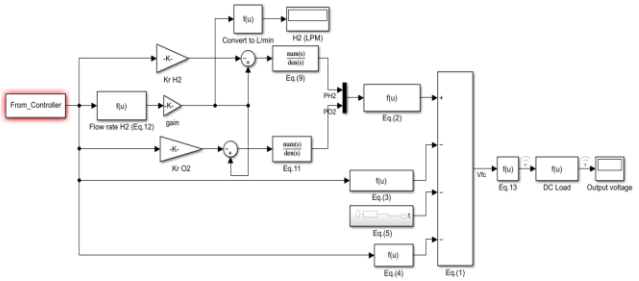

Fig. 4. Simulation model of OC-PEMFC

D. Wavelet Controller

In control systems, signals often contain noise that can affect the performance of the system. Generally, wavelet can be employed for signal denoising by thresholding the detail coefficients [70]. High-frequency noise is often concentrated in the detail coefficients, and by setting small coefficients to zero, the noise can be effectively removed [71]. In this study, biorthogonal Cohen-Daubechies-Feauveau 5/3 (CDF 5/3) wavelets were chosen for their advantageous characteristics, which include the absence of overshoot, a well-balanced frequency response, and minimal delay time [72]. These wavelets are commonly applied in signal processing and image compression [73][74]. Biorthogonal wavelets utilize distinct functions for decomposition (analysis) and reconstruction (synthesis) [75]. The 5 denotes the number of coefficients utilized in both the analysis and synthesis filters, while 3 signifies the number of vanishing moments, influencing the wavelet's smoothness [63]. The analysis and synthesis sequences for CDF 5/3 are provided below. Analysis filters:

$$h(z) = -\frac{1}{8}z^{-2} + \frac{1}{4}z^{-1} + \frac{3}{4} + \frac{1}{4}z^{1} - \frac{1}{8}z^{2} \quad (14)$$

$$g(z) = -\frac{1}{2}z^{-1} + 1 - \frac{1}{2}z^{1} \quad (15)$$

Synthesis filters:

$$\bar{h}(z) = \frac{1}{2}z^{-1} + 1 + \frac{1}{2}z^{1} \quad (16)$$

$$\bar{g}(z) = -\frac{1}{8}z^{-2} - \frac{1}{4}z^{-1} + \frac{3}{4} - \frac{1}{4}z^{1} - \frac{1}{8}z^{2} \quad (17)$$

The following mathematical equation showcases the assessment of repeatability for both the low-pass and high-pass analysis filters within a 5/3 CDF, accounting for the high-pass filter's shift by z^{-1}.

$$h(z) = -\frac{1}{8}z^{-2} + \frac{1}{4}z^{-1} + \frac{3}{4} + \frac{1}{4}z^{1} - \frac{1}{8}z^{2} \quad (18)$$

$$z^{-1}g(z) = z^{-1}\left(-\frac{1}{2}z^{1} - \frac{1}{2}z^{-1} + 1 - \frac{1}{2}z^{1}\right) = \frac{1}{2}z^{-2} + z^{-1} \quad (19)$$

The predict step's coefficient is $\alpha = -1/2$, while for the update step, it's $\beta = -1/4$. Both steps employ the floor function to ensure an integer-to-integer transformation in their equations. Fig. 5 visually depicts the application of the forward CDF 5/3 Discrete Wavelet Transform (DWT) using the lifting scheme.

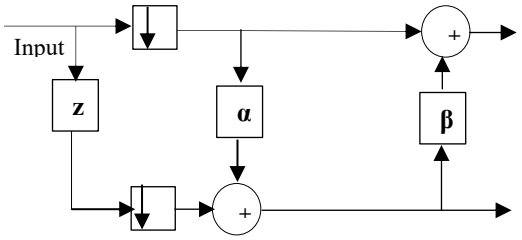

Fig. 5. CDF 5/3 DWT structure using lifting scheme

E. Clipping Technique

The clipping technique functions by constraining amplitude spikes and omitting signal amplitudes beyond a specified threshold [76][77]. This becomes important because using a filter might cause the return of high amplitudes. In mathematical terms, the clipping operation $clip\ (x, a, b)$ for a given value x is expressed as:

$$clip(x, a, b) = \begin{cases} a & if\ x < a \\ x & if\ a \le x \le b \\ b & if\ x > b \end{cases} \quad (20)$$

Where, x is the input signal. a is the lower limit of the range. b is the upper limit of the range.

III. Results and Discussion

A. Fluctuation Findings from Experiments

Fluctuations were noted when applying a 7A current load, although, in reality, the maximum measured current is 6.9 A. Fig. 6 illustrates fluctuations in the load current, ranging from a lower limit of 6.7 A to an upper limit of 6.9 A.

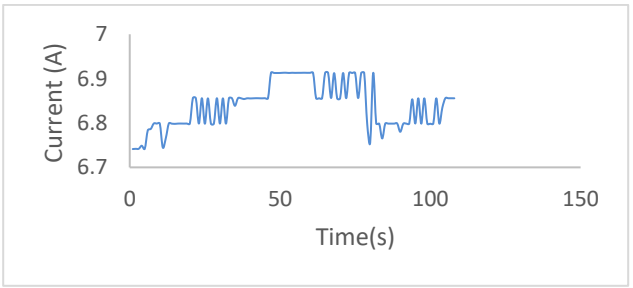

Fig. 6. Fluctuations in load current

The fuel cell output voltage exhibits greater stability at lower current loads, but as the load increases to 7 A, fluctuations in the fuel cell output voltage become apparent can be seen in Fig. 7.

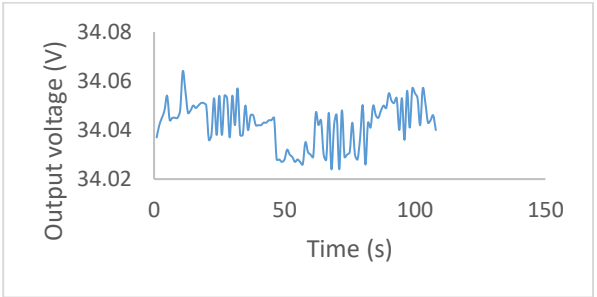

Fig. 7. Fluctuations in output voltage

The variations in output voltage also induce instability in output power, depicted in Fig. 8, with power fluctuating between 229.3 W and 235.3 W.

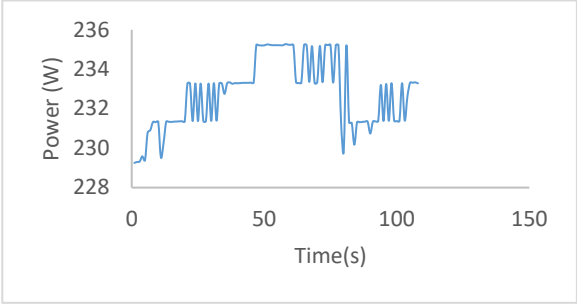

Fig. 8. Fluctuations in output power

B. Validation Fuel Cell Model

Validation involves comparing averaged data from experiments with simulation models. The fuel cell voltage output is measured while gradually increasing the load current from 1 A to 10 A, resulting in the curve depicted in Fig. 9.

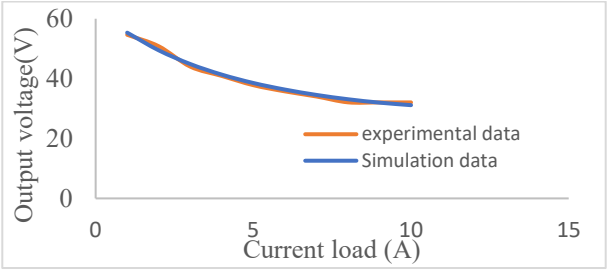

Fig. 9. Experimental and simulation comparison curve for current vs. voltage

In Fig. 9 and Fig. 10, showcasing curves derived from a consistent hydrogen flow input of 8 L/min, the maximum power achieved in experimentation reaches 252.4 W, whereas simulation records a maximum of 260.5 W.

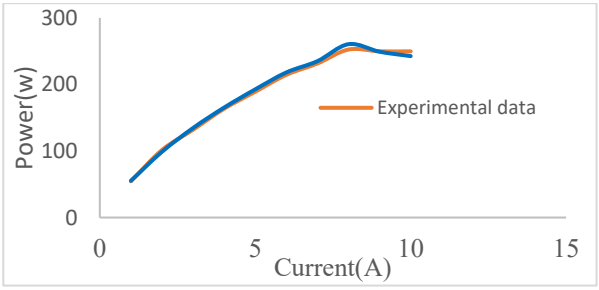

Fig. 10. Experimental and simulation comparison curve for current vs. power

Subsequently, the model is validated using experimental data through the application of equation (21). The equation can compute the relative error (R) between simulation results (V_s) and experimental data (V_e)[26].

$$R = \frac{|V_s - V_e|}{V_e} \quad (21)$$

As per Equation (21), the relative error computed for Fig. 8 stands at 1.8%, and for Fig. 9, it's 1.9%. These findings indicate the fuel cell model's suitability for application

C. Wavelet Clipping Performance Analysis Results

The simulation set point value is set at 6.9 A, aligning with the experimental findings where notable fluctuations commenced. This current is utilized as input in equation (12) to convert it into the hydrogen flow. Subsequently, the fuel cell model employed wavelet clipping. In Fig. 11, the controlled signal contrasts with an uncontrolled signal, demonstrating hydrogen flow fluctuations in the uncontrolled signal, which are stabilized using the proposed method.

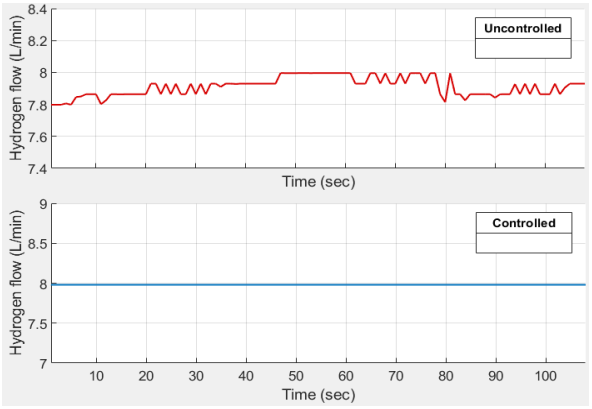

Fig. 11. Comparison of controlled and uncontrolled hydrogen flow

Fig. 11 illustrates the successful application of the wavelet clipping method in stabilizing the hydrogen flow by mitigating uncontrolled fluctuations. Consequently, the hydrogen flow stabilizes at 8.02 L/min, closely approaching the target value of 8 L/min. This indicates a minor deviation between the target and actual values.

The stability of the hydrogen flow directly influences the stability of the output voltage, as depicted in Fig. 12, where the voltage remains stable at 34.704 V. Fuel cell efficiency can be computed using the equation (22) [78].

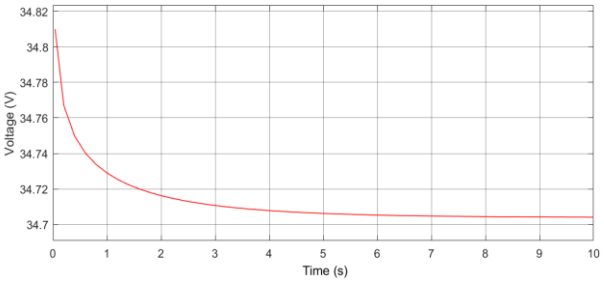

Fig. 12. Output voltage response

$$\eta_{stack} = \frac{V_{cell}}{1.482} \times 100\% \quad (22)$$

By employing equation (22), the average fuel cell efficiency is calculated as 31.5% before the implementation of the wavelet clipping method, as indicated by the graphical data in Fig. 5. Subsequently, after the application of the proposed method, the efficiency shows improvement, reaching 32.1%.

Integral Square Error (ISE) is employed to gauge the cumulative square error between the setpoint and the actual current [79][80]. The Integral Square Error (ISE) serves as an indicator of the accuracy of the control system, with a smaller value signifying higher accuracy.

$$ISE = \int_0^\infty (e(t))^2 dt \quad (23)$$

Utilizing Equation (23), the calculated ISE value is 0.028. This calculation involves comparing the setpoint value (6.9 A) with the actual current value (6.953 A) (the graph for the current response output results can be seen in Fig. 13).

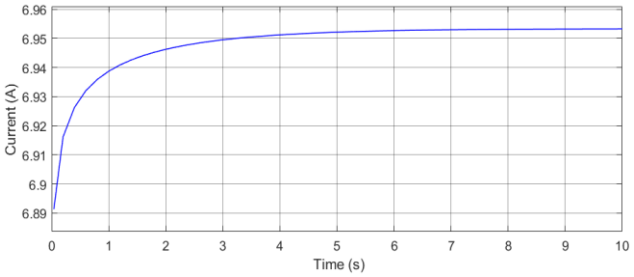

Fig. 13. Output current response

IV. CONCLUSION

The combined wavelet clipping control aims to enhance fuel cell efficiency by ensuring a consistent hydrogen flow under a constant load. This approach is applied to a validated fuel cell model using experimental data, intending to minimize both noise and high amplitude. The key findings from this study are summarized as; 1) The research findings indicate that fluctuations prevent the hydrogen flow into the fuel cell from reaching the target of 8 L/min. Nevertheless, upon implementing the proposed control system, the hydrogen flow stabilizes at 8.02 L/min, with a marginal 0.02 L/min error between the actual and target values. 2) Further investigations reveal that fluctuations in hydrogen flow significantly impact both fuel cell output voltage and efficiency. By mitigating these fluctuations, the fuel cell's efficiency improves from 31.5% to 32.1%, accompanied by a 1.95% increase in output voltage. 3) The evaluation of the proposed control system demonstrates its high accuracy, as evidenced by the low ISE value of 0.028.

In future work, we aim to enhance the performance of Open Cathode PEM fuel cells by incorporating MIMO control techniques to regulate the balance between oxygen and hydrogen flows. The effectiveness of the control is validated through experimental verification for robust performance.

REFERENCES

[1] W. Cardoso, R. Di Felice, and R. C. Baptista, "Mathematical modeling of a solid oxide fuel cell operating on biogas," *Bull. Electr. Eng. Informatics*, vol. 10, no. 6, pp. 2929–2942, Dec. 2021, doi: 10.11591/eei.v10i6.3253.

[2] S. Sharma, S. Agarwal, and A. Jain, "Significance of hydrogen as economic and environmentally friendly fuel," *Energies*, vol. 14, no. 21, 2021, doi: 10.3390/en14217389.

[3] W. Agila, G. Rubio, J. Aviles-Cedeno, and L. Gonzalez, "Approximate Reasoning Techniques in the Control of States of Operation of the PEM Fuel Cell," *11th Int. Conf. Smart Grid, icSmartGrid 2023*, pp. 139–143, 2023, doi: 10.1109/icSmartGrid58556.2023.10170778.

[4] C. Y. Chuang, C. H. Lan, T. S. Lan, X. J. Dai, and J. H. Qin, "Flow control of proton exchange membrane fuel cell with theory of inventive problem solving (TRIZ)," *Sensors Mater.*, vol. 33, no. 5, pp. 1603–1617, May 2021, doi: 10.18494/SAM.2021.3176.

[5] R. Stropnik, N. Mlakar, A. Lotrič, M. Sekavčnik, and M. Mori, "The influence of degradation effects in proton exchange membrane fuel cells on life cycle assessment modelling and environmental impact indicators," *Int. J. Hydrogen Energy*, vol. 47, no. 57, pp. 24223–24241, Jul. 2022, doi: 10.1016/j.ijhydene.2022.04.011.

[6] A. K. Sari *et al.*, "Nata de Cassava Type of Bacterial Cellulose Doped with Phosphoric Acid as a Proton Exchange Membrane," *Membranes*, vol. 13, no. 1, p. 43, 2023.

[7] D. S. Khaerudini *et al.*, "New and Renewable Catalyst Based on Electro-Activated Carbon for Hydrogen Generation," *2019 International Conference on Technologies and Policies in Electric Power & Energy*, pp. 1-6, 2019, doi: 10.1109/IEEECONF48524.2019.9102628..

[8] P. Mandal, B. K. Hong, J. G. Oh, and S. Litster, "Understanding the voltage reversal behavior of automotive fuel cells," *J. Power Sources*, vol. 397, pp. 397–404, Sep. 2018, doi: 10.1016/j.jpowsour.2018.06.083.

[9] D. Yang, R. Pan, Y. Wang, and Z. Chen, "Modeling and control of PEMFC air supply system based on T-S fuzzy theory and predictive control," *Energy*, vol. 188, p. 116078, 2019, doi: 10.1016/j.energy.2019.116078.

[10] X. M. Yuan, F. Ye, J. X. Liu, H. Guo, and C. F. Ma, "Voltage response and two-phase flow during mode switching from fuel cell to water electrolyser in a unitized regenerative fuel cell," *Int. J. Hydrogen Energy*, pp. 15917–15925, Jun. 2019, doi: 10.1016/j.ijhydene.2018.07.017.

[11] Y. Maiket, R. Yeetsorn, and W. Kaewmanee, "Hydrogen Flow Controller Applied to Driving Behavior Observation of Hydrogen Fuel Cell Performance Test," *ACS Omega*, vol. 7, no. 43, pp. 38277–38288, 2022, doi: 10.1021/acsomega.2c02000.

[12] W. Liu, Z. Peng, B. Kim, B. Gao, and Y. Pei, "Development of a PEMFC dynamic model and the application to the analysis of fuel cell vehicle performance," *IOP Conf. Ser. Mater. Sci. Eng.*, vol. 628, no. 1, 2019, doi: 10.1088/1757-899X/628/1/012006.

[13] A. A. J. Jeman, N. M. S. Hannoon, N. Hidayat, M. M. H. Adam, I. Musirin, and V. Vijayakumar, "Experimental study on transient response of fuel cell," *Bull. Electr. Eng. Informatics*, vol. 8, no. 2, pp. 375–381, Jun. 2019, doi: 10.11591/eei.v8i2.1431.

[14] D. N. Luta and A. K. Raji, "Comparing fuzzy rule-based MPPT techniques for fuel cell stack applications," *Energy Procedia*, vol. 156, pp. 177–182, 2019, doi: 10.1016/j.egypro.2018.11.124.

[15] M. Qaiser, A. B. Asghar, M. H. Jaffery, M. Y. Javaid, M. S. Khurram, and L. Campus, "Flow Control Of Hydrogen Fuel In Pem Fuel Cell Using Soft Computing Techniques," *Journal of Ovonic Research*, vol. 17, no. 1, pp. 31–44, 2021.

[16] T. H. Eom, J. W. Kang, J. Kim, M. H. Shin, J. H. Lee, and C. Y. Won, "Improved voltage drop compensation method for hybrid fuel cell battery system," *Electron.*, vol. 7, no. 11, 2018, doi: 10.3390/electronics7110331.

[17] F. S. Nanadegani and B. Sunden, "Review of exergy and energy analysis of fuel cells," *Int. J. Hydrogen Energy*, vol. 48, no. 84, pp. 32875–32942, 2023, doi: 10.1016/j.ijhydene.2023.05.052.

[18] F. Chen, Y. Yu, Y. Liu, and H. Chen, "Control system design for proton exchange membrane fuel cell based on a common rail (I): Control strategy and performance analysis," *Int. J. Hydrogen Energy*, vol. 42, no. 7, pp. 4285–4293, Feb. 2017, doi: 10.1016/j.ijhydene.2016.11.140.

[19] K. Ahmed, O. Farrok, M. M. Rahman, M. S. Ali, M. M. Haque, and A. K. Azad, "Proton exchange membrane hydrogen fuel cell as the grid connected power generator," *Energies*, vol. 13, no. 24, pp. 1–20, 2020, doi: 10.3390/en13246679.

[20] G. I. Applications, "Short Circuit Characteristics of PEM Fuel Cells for Grid Integration Applications," *Electronics*, vol. 9, no. 4, p. 602, 2020, doi: 10.3390/electronics9040602.

[21] M. Dhimish, G. Vieira, and G. Badran, "Investigating the stability and degradation of hydrogen PEM fuel cell," *International Journal of Hydrogen Energy*, vol. 46, no. 74, pp. 37017-37028, 2021, doi: 10.1016/j.ijhydene.2021.08.183.

[22] F. R. Maulana, K. Indriawati, and R. A. Wahyuono, "Reactant Control Strategies for Maximizing Efficiency in Open Cathode PEM Fuel Cell," *Proc. 2023 Int. Conf. Instrumentation, Control. Autom. ICA 2023*, pp. 30–35, 2023, doi: 10.1109/ICA58538.2023.10273067.

[23] D. Huo, Q. Peng, and C. M. Hall, "Koopman-Based Modeling of an Open Cathode Proton Exchange Membrane Fuel Cell Stack," *IFAC-PapersOnLine*, vol. 56, no. 3, pp. 67–72, 2023, doi:

10.1016/j.ifacol.2023.12.002.

[24] C. Zhao, B. Li, L. Zhang, Y. Han, and X. Wu, "Novel optimal structure design and testing of air-cooled open-cathode proton exchange membrane fuel cell," *Renew. Energy*, vol. 215, p. 118899, 2023, doi: 10.1016/j.renene.2023.06.020.

[25] C. Mahjoubi and J. Olivier, "An improved thermal control of open cathode proton exchange membrane fuel cell," *International Journal of Hydrogen Energy*, vol. 44, no. 22, pp. 11332-11345, 2018, doi: 10.1016/j.ijhydene.2018.11.055.

[26] F. Chen, L. Zhang, and J. Jiao, "Modelling of humidity dynamics for open-cathode proton exchange membrane fuel cell," *World Electr. Veh. J.*, vol. 12, no. 3, 2021, doi: 10.3390/wevj12030106.

[27] Z. Guo, C. Tian, K. Gong, W. Xu, L. Chen, and W. Tao, "International Journal of Hydrogen Energy Experimental study on the dynamic response of voltage and temperature of an open-cathode air-cooled proton exchange membrane fuel cell," *International Journal of Hydrogen Energy*, vol. 57, pp. 601–615, 2024.

[28] H. Chen, S. Xu, P. Pei, B. Qu, and T. Zhang, "Mechanism analysis of starvation in PEMFC based on external characteristics," *Int. J. Hydrogen Energy*, vol. 44, no. 11, pp. 5437–5446, Feb. 2019, doi: 10.1016/j.ijhydene.2018.11.135.

[29] J. Li and T. Yu, "Sensors integrated control of PEMFC gas supply system based on large-scale deep reinforcement learning," *Sensors (Switzerland)*, vol. 21, no. 2, pp. 1–19, Jan. 2021, doi: 10.3390/s21020349.

[30] X. Bai and Q. Jian, "Decoupling strategy for react-air supply and cooling of open-cathode proton exchange membrane fuel cell stack considering real-time membrane resistance estimation," *J. Clean. Prod.*, vol. 410, p. 137288, 2023, doi: 10.1016/j.jclepro.2023.137288.

[31] X. Zhu *et al.*, "Performance analysis of proton exchange membrane fuel cells with traveling-wave flow fields based on Grey-relational theory," *Int. J. Hydrogen Energy*, vol. 48, no. 2, pp. 740–756, 2023, doi: 10.1016/j.ijhydene.2022.09.244.

[32] M. Bressel, M. Hilairet, D. Hissel, and B. Ould Bouamama, "Model-based aging tolerant control with power loss prediction of Proton Exchange Membrane Fuel Cell," *Int. J. Hydrogen Energy*, vol. 45, no. 19, pp. 11242–11254, 2020, doi: 10.1016/j.ijhydene.2018.11.219.

[33] M. Obermaier, M. Rauber, A. Bauer, T. Lochner, F. Du, and C. Scheu, "Local Fuel Starvation Degradation of an Automotive PEMFC Full Size Stack," *Fuel Cells*, vol. 20, no. 4, pp. 394–402, Aug. 2020, doi: 10.1002/fuce.201900180.

[34] L. Xia, M. Ni, Q. He, Q. Xu, and C. Cheng, "Optimization of gas diffusion layer in high temperature PEMFC with the focuses on thickness and porosity," *Appl. Energy*, vol. 300, p. 117357, 2021, doi: 10.1016/j.apenergy.2021.117357.

[35] H. A. Dhahad, W. H. Alawee, and A. K. Hassan, "Experimental study of the effect of flow field design to PEM fuel cells performance," *Renew. Energy Focus*, vol. 30, pp. 71–77, 2019, doi: 10.1016/j.ref.2019.05.002.

[36] Y. Qi, M. Thern, M. Espinoza-Andaluz, and M. Andersson, "Modeling and Control Strategies of Proton Exchange Membrane Fuel Cells," in *Energy Procedia*, vol. 159, pp. 54–59, 2019, doi: 10.1016/j.egypro.2018.12.017.

[37] F. Jia, X. Tian, F. Liu, J. Ye, and C. Yang, "Oxidant starvation under various operating conditions on local and transient performance of proton exchange membrane fuel cells," *Appl. Energy*, vol. 331, p. 120412, 2023, doi: 10.1016/j.apenergy.2022.120412.

[38] M. Fattahi, "Fuzzy sliding mode control of hydrogen flow in PEM fuel cell system for residential power generation," *2017 5th International Conference on Control, Instrumentation, and Automation (ICCIA)*, pp. 1-6, 2017, doi: 10.1109/ICCIAutom.2017.8373943..

[39] W. Wang, J. Chen, C. Xiao, and N. Cheng, "Adaptive fuzzy control method of hydrogen fuel cell gas supply system," *J. Phys. Conf. Ser.*, vol. 1983, no. 1, 2021, doi: 10.1088/1742-6596/1983/1/012051.

[40] Y. B. Yakut, "A new control algorithm for increasing efficiency of PEM fuel cells – Based boost converter using PI controller with PSO method," *Int. J. Hydrogen Energy*, 2023, doi: 10.1016/j.ijhydene.2023.12.008.

[41] Y. Huang and Y. Huang, "Research on PID Parameter Self-Tuning Speed Control System Based on Grasshopper Optimazation Algorithm-Optimized BP Neural Network," *2023 3rd Int. Conf. Energy, Power Electr. Eng.*, pp. 1444–1450, 2023, doi: 10.1109/epee59859.2023.10351813.

[42] F. Behrooz, N. Mariun, M. H. Marhaban, M. A. M. Radzi, and A. R. Ramli, "Review of control techniques for HVAC systems-nonlinearity approaches based on fuzzy cognitive maps," *Energies*, vol. 11, no. 3, 2018, doi: 10.3390/en11030495.

[43] N. A. Zambri, N. Bin Salim, F. H. M. Noh, and S. S. Yi, "Performance comparison of PEMFC hydrogen reformer with different controllers," *Telkomnika (Telecommunication Comput. Electron. Control.*, vol. 17, no. 5, pp. 2617–2624, 2019, doi: 10.12928/TELKOMNIKA.v17i5.12817.

[44] N. Rifai, J. Sabor, and C. Alaoui, "PEM Fuel Cell Dynamic Modeling Based On Transfer Functions," *2022 2nd Int. Conf. Innov. Res. Appl. Sci. Eng. Technol. IRASET 2022*, pp. 1–5, 2022, doi: 10.1109/IRASET52964.2022.9738273.

[45] X. Hou *et al.*, "Energy, economic, and environmental analysis: A study of operational strategies for combined heat and power system based on PEM fuel cell in the East China region," *Renew. Energy*, vol. 223, p. 120023, 2024, doi: 10.1016/j.renene.2024.120023.

[46] W. Andari, S. Ghozzi, M. S. Ben Yahia, H. Allagui, and A. Mami, "Supervisory control design for a PEM fuel cell electric vehicle," *2021 12th Int. Renew. Energy Congr. IREC 2021*, pp. 21–25, 2021, doi: 10.1109/IREC52758.2021.9624829.

[47] C. Mahjoubi, J. C. Olivier, S. Skander-mustapha, M. Machmoum, and I. Slama-belkhodja, "An improved thermal control of open cathode proton exchange membrane fuel cell," *Int. J. Hydrogen Energy*, vol. 44, no. 22, pp. 11332–11345, 2019, doi: 10.1016/j.ijhydene.2018.11.055.

[48] Y. Cao, Y. Li, G. Zhang, K. Jermsittiparsert, and N. Razmjooy, "Experimental modeling of PEM fuel cells using a new improved seagull optimization algorithm," *Energy Reports*, vol. 5, pp. 1616–1625, 2019, doi: 10.1016/j.egyr.2019.11.013.

[49] M. Bayat and M. Özalp, "Effects of leak current density and doping level on energetic, exergetic and ecological performance of a high-temperature PEM fuel cell," *Int. J. Hydrogen Energy*, vol. 48, no. 60, pp. 23212–23229, 2023, doi: 10.1016/j.ijhydene.2023.03.277.

[50] P. Xie, S. S. Araya, J. M. Guerrero, and J. C. Vasquez, "Dynamic Modeling and Control of High Temperature PEM Fuel Cell and Battery System for Electrical Applications," *IECON Proc. (Industrial Electron. Conf.*, pp. 1–6, 2023, doi: 10.1109/IECON51785.2023.10312306.

[51] J. Kuang *et al.*, "Oxygen excess ratio control of PEM fuel cell systems with prescribed regulation time," *ISA Trans.*, vol. 142, pp. 683–692, 2023, doi: 10.1016/j.isatra.2023.07.026.

[52] K. Benmouiza and A. Cheknane, "Analysis of proton exchange membrane fuel cells voltage drops for different operating parameters," *Int. J. Hydrogen Energy*, vol. 43, no. 6, pp. 3512–3519, Feb. 2018, doi: 10.1016/j.ijhydene.2017.06.082.

[53] B. O. Emmanuel, P. Barendse, and J. Chamier, "Effect of Anode Stoichiometry and Back Pressure on the Performance of PEMFCs," *2018 IEEE PES/IAS PowerAfrica, PowerAfrica 2018*, pp. 1–6, 2018, doi: 10.1109/PowerAfrica.2018.8521183.

[54] X. Li, J. Wang, W. Huang, and H. Dong, "Fuzzy Adaptive Algorithm Controls Oxygen Excess Coefficient of Air Blower and System Net Power of Proton Exchange Membrane Fuel Cell," *2023 7th Int. Conf. Smart Grid Smart Cities, ICSGSC 2023*, pp. 343–348, 2023, doi: 10.1109/ICSGSC59580.2023.10319237.

[55] F. Z. Amatoul and M. Er-raki, "Modeling and simulation of electrical generation systems based on PEM fuel cell-boost converter using a closed loop PI controller," *Energy Reports*, vol. 9, no. S11, pp. 296–308, 2023, doi: 10.1016/j.egyr.2023.08.055.

[56] M. Zadehbagheri, M. J. Kiani, and T. Sutikno, "Investigation of the Effects of Fuel Cells on V-Q & V-P Characteristics," *J. Robot. Control*, vol. 3, no. 4, pp. 535–545, 2022, doi: 10.18196/jrc.v3i4.14855.

[57] S. Cheng *et al.*, "Investigation and analysis of proton exchange membrane fuel cell dynamic response characteristics on hydrogen consumption of fuel cell vehicle," *Int. J. Hydrogen Energy*, vol. 47, no. 35, pp. 15845–15864, 2022, doi: 10.1016/j.ijhydene.2022.03.063.

[58] B. Li, Z. Guo, L. Zeng, J. Fu, C. Sheng, and X. Li, "Optimization of Parameter Matching for PEM Fuel Cell Hybrid Power System," *Chinese Control Conf. CCC*, pp. 6340–6345, 2023, doi: 10.23919/CCC58697.2023.10240722.

[59] U. K. Chakraborty, "A New Model for Constant Fuel Utilization and

Constant Fuel Flow in Fuel Cells," *Appl. Sci.*, vol. 9, no. 6, 2019, doi: 10.3390/app9061066.

[60] A. Elbaz, M. H. Elfar, A. Kalas, and A. Refaat, "Maximum Power Extraction from Polymer Electrolyte Membrane (PEM) Fuel Cell Based on Deterministic Particle Swarm Optimization Algorithm," *Proc. 2022 Conf. Russ. Young Res. Electr. Electron. Eng. ElConRus 2022*, pp. 613–619, 2022, doi: 10.1109/ElConRus54750.2022.9755807.

[61] M. Li, M. Lin, L. Wang, Y. Wang, F. Pan, and X. Zhao, "Observation and Analysis of Ejector Hysteresis Phenomena in the Hydrogen Recirculation Subsystem of PEMFCs," *Entropy*, vol. 25, no. 3, p. 426, 2023, doi: 10.3390/e25030426.

[62] S. and A. K. Darjat , Sulistyo, Aris Triwiyatno, "Designing Hydrogen and Oxygen Flow Rate Control on a Solid Oxide Fuel Cell Simulator Using the Fuzzy Logic Control Method," *Process*, vol. 8, no. 154, pp. 1–22, 2020.

[63] K. Mammar, F. Saadaoui, and A. Hazzab, "Development and simulation of a PEM fuel cell model for prediction of water content and power generation," vol. 4, no. 2017, pp. 289–299, 2018, doi: 10.22104/ijhfc.2018.2792.1168.

[64] X. Tang, Y. Zhang, and S. Xu, "Experimental study of PEM fuel cell temperature characteristic and corresponding automated optimal temperature calibration model," *Energy*, vol. 283, p. 128456, 2023, doi: 10.1016/j.energy.2023.128456.

[65] E. A. El-Hay, M. A. El-Hameed, and A. A. El-Fergany, "Optimized Parameters of SOFC for steady state and transient simulations using interior search algorithm," *Energy*, vol. 166, pp. 451–461, 2019, doi: 10.1016/j.energy.2018.10.038.

[66] N. Benchouia, A. E. Hadjadj, A. Derghal, L. Khochemane, and B. Mahmah, "Modeling and validation of fuel cell PEMFC," *J. Renew. Energies*, vol. 16, no. 2, pp. 365–377, 2023, doi: 10.54966/jreen.v16i2.386.

[67] M. Y. Silaa, O. Barambones, and A. Bencherif, "A Novel Adaptive PID Controller Design for a PEM Fuel Cell Using Stochastic Gradient Descent with Momentum Enhanced by Whale Optimizer," *Electron.*, vol. 11, no. 16, 2022, doi: 10.3390/electronics11162610.

[68] M. Derbeli, M. Farhat, O. Barambones, and L. Sbita, "Control of PEM fuel cell power system using sliding mode and super-twisting algorithms," *Int. J. Hydrogen Energy*, vol. 42, no. 13, pp. 8833–8844, 2017, doi: 10.1016/j.ijhydene.2016.06.103.

[69] N. Rifai, J. Sabor, C. Alaoui, R. Petrone, and H. Gualous, "Dynamic modeling of an open cathode PEM fuel cell for automotive energy management applications," *Int. J. Power Electron. Drive Syst.*, vol. 13, no. 3, pp. 1406–1418, 2022, doi: 10.11591/ijpeds.v13.i3.pp1406-1418.

[70] M. A. Khan, A. Haque, V. S. B. Kurukuru, and F. Blaabjerg, "Optimizing the Performance of Single-Phase Photovoltaic Inverter using Wavelet-Fuzzy Controller," *e-Prime - Adv. Electr. Eng. Electron. Energy*, vol. 3, p. 100093, 2023, doi: 10.1016/j.prime.2022.100093.

[71] A. K. Samantaray, P. Gorre, and P. K. Sahoo, "Design of CSD based bi-orthogonal wavelet filter bank for medical image retrieval," *e-Prime - Adv. Electr. Eng. Electron. Energy*, vol. 5, p. 100242, 2023, doi: 10.1016/j.prime.2023.100242.

[72] M. Sushmitha, S. Chetan, and S. Sarkar, "An Efficient High-Speed Lifting Based 1D/2D-DWT VLSI Architecture Using CDF-5/3 Wavelet Transform for Image Processing Applications," *Proc. - 5th IEEE Int. Conf. Recent Trends Electron. Inf. Commun. Technol. RTEICT 2020*, pp. 269–274, 2020, doi: 10.1109/RTEICT49044.2020.9315649.

[73] M. Sushmitha, S. Chetan and S. Sarkar, "An Efficient High-Speed Lifting Based 1D/2D-DWT VLSI Architecture Using CDF-5/3 Wavelet Transform For Image Processing Applications," *2020 International Conference on Recent Trends on Electronics, Information, Communication & Technology (RTEICT)*, pp. 269-274, 2020, doi: 10.1109/RTEICT49044.2020.9315649.

[74] M. Gholipour, "Design and implementation of lifting based integer wavelet transform for image compression applications," *Commun. Comput. Inf. Sci.*, vol. 166, pp. 161–172, 2011, doi: 10.1007/978-3-642-21984-9_14.

[75] S. Krishna, D. Kumar, and V. K. Dwivedi, "Biorthogonal Wavelets for Multiresolution Image Compression," *2022 2nd Int. Conf. Power Electron. IoT Appl. Renew. Energy its Control. PARC 2022*, pp. 1–7, 2022, doi: 10.1109/PARC52418.2022.9726558.

[76] B. Bakkas, R. Benkhouya, I. Chana, and H. Ben-azza, "Palm Date Leaf Clipping : A New Method to Reduce PAPR in OFDM Systems," *Information*, vol. 11, no. 4, p. 190, 2020.

[77] B. Tang, K. Qin, and C. Chen, "A Novel Clipping-Based Method to Reduce Peak-To-Average Power Ratio of OFDM Signals," *Information*, vol. 11, no. 2, p. 113, 2020.

[78] W. Pirom and A. Srisiriwat, "Experimental Study of Hybrid Photovoltaic-PEM Electrolyzer-PEM Fuel Cell System," *Proc. 2022 Int. Electr. Eng. Congr. iEECON 2022*, pp. 1–4, 2022, doi: 10.1109/iEECON53204.2022.9741687.

[79] Z. Baroud, A. Benalia, and C. Ocampo-Martinez, "Air flow regulation in fuel cells: An efficient design of hybrid fuzzy-PID control," *EEA - Electroteh. Electron. Autom.*, vol. 64, no. 4, pp. 28–32, 2016.

[80] Z. Baroud, M. Benmiloud, A. Benalia, and C. Ocampo-Martinez, "Novel hybrid fuzzy-PID control scheme for air supply in PEM fuel-cell-based systems," *Int. J. Hydrogen Energy*, vol. 42, no. 15, pp. 10435–10447, 2017, doi: 10.1016/j.ijhydene.2017.01.014.